

Crossover between different regimes of inhomogeneous superconductivity in planar superconductor–ferromagnet hybrids

A.Yu. Aladyshkin,^{1,2} J. Fritzsche,¹ R. Werner,³ R.B.G. Kramer,^{1,4}
S. Guénon,³ R. Kleiner,³ D. Koelle,³ and V.V. Moshchalkov¹

¹*INPAC – Institute for Nanoscale Physics and Chemistry,
K.U. Leuven, Celestijnenlaan 200D, B-3001 Leuven, Belgium*

²*Institute for Physics of Microstructures RAS, 603950, Nizhny Novgorod, GSP-105, Russia*

³*Physikalisches Institut – Experimentalphysik II, Universität Tübingen,
Auf der Morgenstelle 14, 72076 Tübingen, Germany*

⁴*Institut Néel, CNRS–Université Joseph Fourier, BP 166, 38042 Grenoble Cedex 9, France*

(Dated: May 6, 2019)

We studied experimentally the effect of a stripe-like domain structure in a ferromagnetic BaFe₁₂O₁₉ substrate on the magnetoresistance of a superconducting Pb microbridge. The system was designed in such a way that the bridge is oriented perpendicular to the domain walls. It is demonstrated that depending on the ratio between the amplitude of the nonuniform magnetic field B_0 , induced by the ferromagnet, and the upper critical field H_{c2} of the superconducting material, the regions of the reverse-domain superconductivity in the $H - T$ plane can be isolated or can overlap (H is the external magnetic field, T is temperature). The latter case corresponds to the condition $B_0/H_{c2} < 1$ and results in the formation of superconductivity above the magnetic domains of both polarities. We discovered the regime of edge-assisted reverse-domain superconductivity, corresponding to localized superconductivity near the edges of the bridge above the compensated magnetic domains. Direct verification of the formation of inhomogeneous superconducting states and external-field-controlled switching between normal state and inhomogeneous superconductivity were obtained by low-temperature scanning laser microscopy.

PACS numbers: 74.25.F- 74.25.Sv 74.25.Op 74.78.-w 74.78.Na

I. INTRODUCTION

Recent advances in fabrication technology have made it possible to realize superconductor–ferromagnet (S/F) hybrid structures with a controlled arrangement of the ferromagnetic layers/elements. These flux–coupled and exchange–coupled S/F hybrids^{1–4} are of fundamental interest for investigations of the nontrivial interaction between superconductivity and a nonuniform distribution of a local magnetic field (or magnetization). Furthermore, S/F hybrids seem to be potential candidates for the development of tunable elements of superconducting electronics.⁴ In this paper we focus only on the planar S/F structures, consisting of a low- T_c superconducting film and a ferromagnetic layer with a domain structure with a dominant magnetostatic interaction between superconducting and ferromagnetic films.^{5–30}

The nonuniform component of the magnetic field, induced by a ferromagnet, can modify the conditions for the appearance of superconductivity in thin superconducting films due to the effect of field compensation. The formation of localized superconductivity in the areas of compensated magnetic field^{31–33} results in an exotic dependence of the superconducting critical temperature T_c on the external magnetic field H , applied perpendicular to the thin film plane. This phase transition line T_c vs. H for planar S/F hybrids becomes non-monotonous^{5–17,32–35} and thus, it differs significantly from the standard linear dependence of the upper critical

field H_{c2} on temperature T , which can be written as

$$1 - \frac{T_c}{T_{c0}} = \frac{|H|}{H_{c2}^{(0)}}. \quad (1)$$

Here T_{c0} is the critical temperature of the superconducting transition at zero magnetic field, $H_{c2}^{(0)} = \Phi_0/(2\pi\xi_0^2)$ and ξ_0 are upper critical field and coherence length at $T = 0$, respectively, and $\Phi_0 = \pi\hbar c/e$ is the magnetic flux quantum. Such dependence given by Eq. (1) is inherent for plain superconducting films in a uniform magnetic field H and shown by the dashed line in Fig. 1.

Considering qualitatively the effect of an inhomogeneous magnetic field, which varies periodically from $+B_0$ (above positive magnetic domains) to $-B_0$ (above negative domains) and remains constant inside the domains, one can expect two different phase transition lines

$$1 - \frac{T_c^{(+)}}{T_{c0}} = \frac{|H + B_0|}{H_{c2}^{(0)}}, \quad (\text{positive domains}), \quad (2)$$

$$1 - \frac{T_c^{(-)}}{T_{c0}} = \frac{|H - B_0|}{H_{c2}^{(0)}}, \quad (\text{negative domains}). \quad (3)$$

These two different transition lines correspond to the formation of superconductivity in the areas where the perpendicular z –component of the nonuniform magnetic field is positive, Eq. (2), or negative, Eq. (3). The phase diagram $H - T$, composed according to Eqs. (2)–(3), is shown in Fig. 1. An inhomogeneous superconducting state trapped only within the areas above the

domains of the opposite polarity with respect to the sign of H , is commonly referred to as reverse-domain superconductivity (RDS).^{8–12,34} In order to guarantee the formation of such RDS exclusively above either positive domains (at $H < 0$) or above negative domains (at $H > 0$), one should satisfy $B_0/H_{c2} > 1$ (i.e., at high temperatures or/and large B_0 values). Such separated regions of RDS above the domains of different signs were observed experimentally^{10–14,18} for Pb/BaFe₁₂O₁₉, Nb/BaFe₁₂O₁₉ and Al/BaFe₁₂O₁₉ hybrid structures. Upon decreasing T and/or B_0 , inhomogeneous superconductivity above magnetic domains of both polarities (i.e. parallel and antiparallel) can coexist (cf. Fig. 1), since both criteria for the formation of inhomogeneous superconductivity above both magnetic domains, $|H - B_0| < H_{c2}$ and $|H + B_0| < H_{c2}$, can be fulfilled simultaneously — provided

$$-\left(1 - \frac{B_0}{H_{c2}}\right) < \frac{H}{H_{c2}} < \left(1 - \frac{B_0}{H_{c2}}\right). \quad (4)$$

The threshold temperature T^* of the crossover from simple RDS to a complex state consisting of RDS in the compensated regions and parallel domain superconductivity (PDS) in the regions with enhanced magnetic field corresponds to the intersection point of the dependencies $T_c^{(+)}(H)$ and $T_c^{(-)}(H)$ at $H = 0$ and can be estimated as $T^* = T_{c0}(1 - B_0/H_{c2})$. Such an inhomogeneous superconducting state, potentially observed in the H range described by Eq. (4) and characterized by a development of superconductivity above magnetic domains of both polarities, can be also called complete superconductivity (CS).

For superconducting samples of finite lateral dimensions one can expect the appearance of surface superconductivity,^{36,37} i.e. superconductivity localized near the sample edges even in the presence of a nonuniform magnetic field. In the first approximation, the phase transition line for such anticipated edge-assisted (EA) superconductivity can be described by the shifted H_{c3} dependencies

$$1 - \frac{T_c^{(\pm)}}{T_{c0}} = 0.59 \frac{|H \pm B_0|}{H_{c2}^{(0)}}, \quad (5)$$

where the signs $+/-$ correspond to edge-assisted superconductivity above positive/negative magnetic domains, respectively. This means that superconductivity near the sample's edges will survive until the local field exceeds the critical field of surface superconductivity $H_{c3} = 1.69 H_{c2}$. Furthermore, the presence of the domain walls stimulates the formation of domain-wall superconductivity (DWS) for moderate fields, $|H| \leq B_0$.^{33,35} It has been shown that for thin superconducting films (in the (x, y) plane) in a perpendicular magnetic field $B_z = H + b_z(x)$ with a step-like component $b_z(x) = B_0 \text{sign}(x)$ induced by a domain wall, nucleation of the superconducting order parameter along the domain wall (at $x = 0$) becomes possible below the phase transition line³⁸

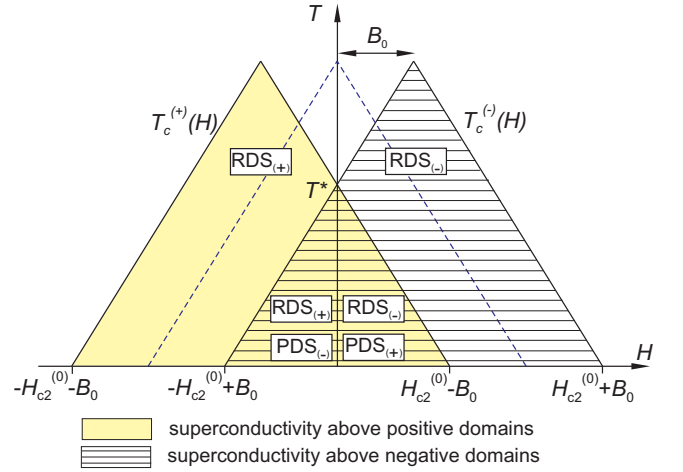


FIG. 1: (color online) Transformation of the phase diagram “external magnetic field (H) – temperature (T)” in the presence of a nonuniform magnetic field (B_0 is the amplitude of the z -component of the stray field). The dashed line is plotted according to Eq. (1). The filled (shaded) area corresponds to inhomogeneous superconductivity above positive and negative magnetic domains, respectively, see Eqs. (2)–(3). Here we use the notations: $RDS_{(\pm)}$ – reverse-domain superconductivity localized above positive (+) domains at $H < 0$ and above negative (–) domains at $H > 0$; $PDS_{(\pm)}$ – parallel-domain superconductivity localized above positive (+) domains at $H > 0$ and above negative (–) domains at $H < 0$.

$$1 - \frac{T_c^{DWS}}{T_{c0}} \simeq \frac{B_0}{H_{c2}^{(0)}} \times \left\{ 0.59 - 0.70 \left(\frac{H}{B_0}\right)^2 + 0.09 \left(\frac{H}{B_0}\right)^4 \right\}. \quad (6)$$

Thus, the set of possible nonuniform superconducting solutions in flux-coupled S/F hybrids has to include the following states: domain-wall superconductivity (DWS), “bulk” RDS and PDS above either positive or negative domains, edge-assisted RDS and PDS above either positive or negative domains, and CS above the domains of both polarities.

In this paper we present an experimental study of the temperature- and field-induced crossover between the different regimes of bulk and localized superconductivity in S/F hybrid structures, consisting of a thin superconducting Pb film on top of a bulk ferromagnetic BaFe₁₂O₁₉ single crystal with a well defined stripe-like domain structure. In order to exclude percolation effects and electrical shunting arising from different superconducting states, we prepared the hybrid S/F structure such that the domain walls are oriented *across* the superconducting microbridge. As a result, the current density is distributed over the entire cross-section of the microbridge, what allows us to detect variations of the voltage drop associated with the appearance/destruction of inhomogeneous

superconductivity of various types.

II. MAGNETIC PROPERTIES OF THE FERROMAGNETIC SUBSTRATE

For the creation of a static nonuniform magnetic field with a well-defined domain structure, we used bulk ferromagnetic crystals $\text{BaFe}_{12}\text{O}_{19}$ (BFO). When cut along the proper crystallographic direction, these BFO crystals exhibit a stripe-type domain structure with dominant in-plane magnetization and a relatively small out-of-plane component of magnetization.^{12–14,18}

Measurements with a vibrating sample magnetometer revealed that at low temperatures the magnetization of the used crystal depends almost linearly on the applied perpendicular magnetic field, and that it saturates at $H \simeq 17$ kOe (see Fig. 2). This means that external magnetic field $|H| \leq 1.5$ kOe, which corresponds to the range of the H -sweeps in our measurements, can only be of minor influence on the domain structure, since the variation of magnetization of the substrate is expected to be not more than 4.5% of the saturated magnetization.

The spatial two-dimensional (2D) distribution of the perpendicular z -component of the magnetic field b_z , induced by the laminar domain structure, was imaged with a scanning Hall probe microscope³⁹ (Fig. 3). By analyzing the 2D patterns of $b_z(x, y)$, which corresponds to the difference between the locally measured field $B_z(x, y)$ of the crystals and the external magnetic field H [panels (a)–(b)], we come to the following conclusions:

- (i) the domain walls remain rectilinear even in the presence of an external field;
- (ii) the effect of the external field is limited mainly to a small displacement of the domain walls as H varies, leading to a broadening of the positive magnetic domains at $H > 0$ at the expense of the negative magnetic domains, and vice versa.

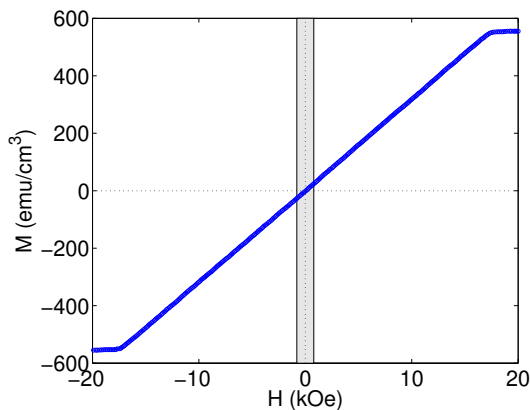


FIG. 2: (color online) Magnetization curve M vs. H , obtained with a vibrating sample magnetometer at $T = 5$ K. The shaded area indicates the range of H in our experiment.

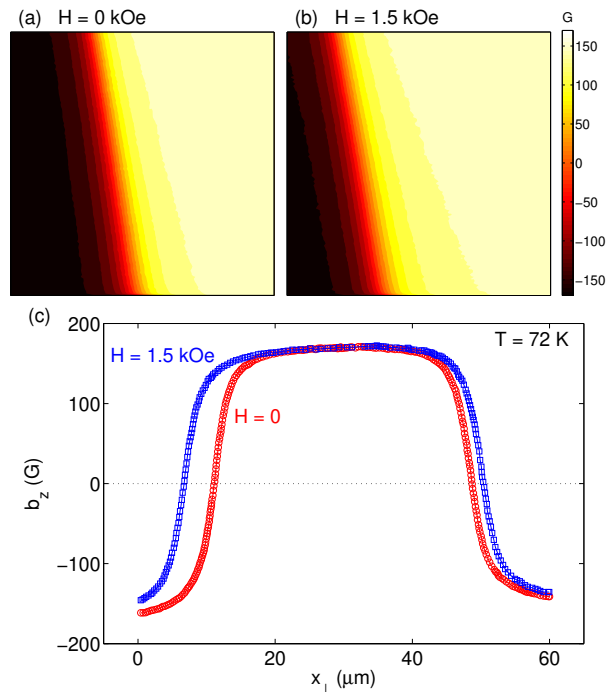


FIG. 3: (Color online) (a)–(b) Two-dimensional distribution of the z -component of the nonuniform magnetic field $b_z(x, y) = B_z(x, y) - H$ measured near a domain wall by a scanning Hall probe microscope at the distance 400 nm above the ferromagnetic crystal at the external magnetic field $H = 0$ (a) and $H = 1.5$ kOe (b) at $T = 72$ K. The scanning area is $35 \mu\text{m} \times 35 \mu\text{m}$.

(c) One-dimensional profile of the nonuniform magnetic field $b_z(x_\perp) = B_z(x_\perp) - H$ along the direction perpendicular to two domain walls, measured by a scanning Hall probe microscope for the same conditions: $H = 0$ (red circles) and $H = 1.5$ kOe (blue squares).

The 1D profile of the stray field b_z along a line perpendicular to the domain walls is shown in Fig. 3(c). We find that an external field of the order of 1 kOe shifts the points $b_z \simeq 0$ at maximum $3 \mu\text{m}$, which is much less than the equilibrium domain width of $30 \mu\text{m}$, without substantial changes in both the shape of the domain wall and the amplitude of the built-in magnetic field. This allows us to consider the field pattern as almost independent on H .

III. SUPERCONDUCTING PROPERTIES OF THE S/F BILAYER

Sample preparation. After polishing the cut-surfaces of the BFO crystals, we prepared lithographically an array of metallic Au markers ($2 \times 2 \mu\text{m}$ in size) on top of the ferromagnetic template. The location of the domain walls with respect to the periodically positioned Au markers was determined with a magnetic force microscope (MFM) at room temperature. A thin insulating Ge layer (4 nm thick) was evaporated in order to prevent

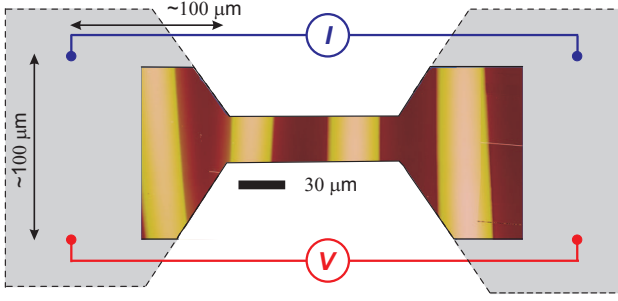


FIG. 4: (color online) Combined MFM and optical image of the short Pb thin film bridge fabricated on top of the BFO single crystal. The alternating dark and bright stripes, corresponding to the magnetic domains with different orientation of the magnetic moment, are shown only within the superconducting bridge. All elements of the electrical circuit as well as the geometry of the contact pads (grey areas) are shown schematically.

exchange interaction and proximity effect between the superconducting and ferromagnetic layers. Finally, two Pb bridges oriented *across* the domain walls were fabricated by means of e-beam lithography, molecular beam epitaxy and lift-off technique in a single run on the same substrate. These superconducting bridges have the same width ($30\ \mu\text{m}$) and thickness ($40\ \text{nm}$) and differ only by their lengths: $100\ \mu\text{m}$ for the short bridge and $700\ \mu\text{m}$ for the long bridge, resulting in different numbers of domain walls (4 and 24, respectively) in the narrow part of the bridges. A combination of an optical and an MFM image of the short Pb bridge is presented in Fig. 4.

Magnetoresistive curves $R(H)$. Measurements of the dc electrical resistance R of both the short and the long superconducting Pb bridges as a function of temperature T , H (applied perpendicularly to the plane of the structures) and the bias current I , were carried out in a commercial Oxford Instruments cryostat using a conventional four-terminal configuration.

Typical $R(H)$ curves measured at $I = 100\ \mu\text{A}$ are shown in Fig. 5(a). The appearance of two symmetrical minima in $R(H)$ at $T = 7.20\ \text{K}$ corresponds to RDS above the domains of opposite polarity. Taking the positions of the R minima, one can estimate the amplitude of the nonuniform magnetic field B_0 inside the superconducting bridge to $480\ \text{Oe}$. The observed linear increase in the width of the R minima with decreasing temperature (compare the curves from $T = 7.20\ \text{K}$, and to $6.50\ \text{K}$) allows us to prove the usual relationship $H_{c2} = H_{c2}^{(0)} (1 - T/T_{c0})$ (Eq. 1) and to estimate both the maximal critical temperature $T_{c0} = 7.25\ \text{K}$ and $H_{c2}^{(0)} \simeq 2.25 \times 10^3\ \text{Oe}$. Contrary to the previously studied hybrid Al/BaFe₁₂O₁₉ bilayers,^{12–14} the estimated $H_{c2}^{(0)}$ value for Pb is substantially higher than B_0 at low temperatures. The ratio $B_0/H_{c2}^{(0)} \simeq 0.2$ gives us the temperature of the anticipated crossover $T^* = 5.70\ \text{K}$ be-

tween RDS and CS. The $R(H)$ at $T = 5.70\ \text{K}$ confirms this simple estimate since the sample resistance vanishes for $T < 5.70\ \text{K}$ at $H = 0$ which indicates CS.

Considering the $R(H)$ curves at rather low temperatures ($T < T^*$), one can see that the transition from the superconducting to the normal state upon increasing $|H|$ from zero occurs in two stages. The first stage and an appearance of nonzero resistance can be attributed to the suppression of bulk PDS above the parallel domains since the position of this anomaly corresponds to Eqs. (2)–(3). However, due to the presence of a continuous superconducting path along the sample edges attributed to edge-assisted superconductivity (PDS), the resistance increases slowly as H increases. The exclusive survival of RDS above opposite domains at larger H explains the rise in the total sample's resistance R up to 50–60% from the normal state resistance R_n (curves $4.50\ \text{K}$, $4.90\ \text{K}$, $5.30\ \text{K}$ and $5.70\ \text{K}$). Indeed, for the considered topology of the magnetic field, the superconducting and normal regions are connected in series and, therefore, R should reflect the ratio between the volume of the bridge in the

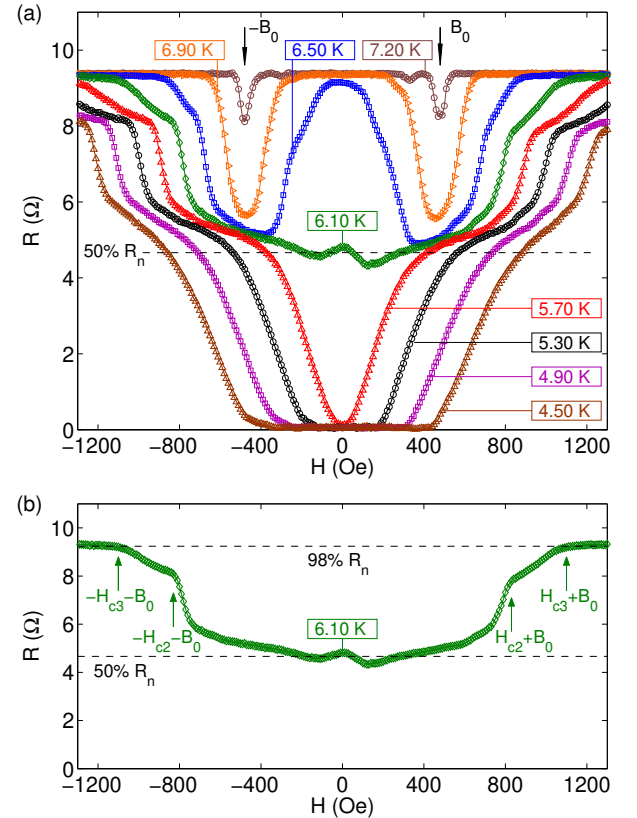


FIG. 5: (Color online) (a) Typical dependencies R vs. H taken for the long Pb microbridge at a fixed bias current $I = 100\ \mu\text{A}$ and at different temperatures T .

(b) A single resistive $R(H)$ curve at $6.10\ \text{K}$ and the position of the critical fields $|H_{c2} + B_0|$ and $|H_{c3} + B_0|$, marked by arrows: $B_0 \simeq 480\ \text{Oe}$, $H_{c2} \simeq 350\ \text{Oe}$, $H_{c3} \simeq 620\ \text{Oe}$. Two dashed horizontal lines show the levels $0.50 R_n$ and $0.98 R_n$, where $R_n \approx 9.55\ \Omega$.

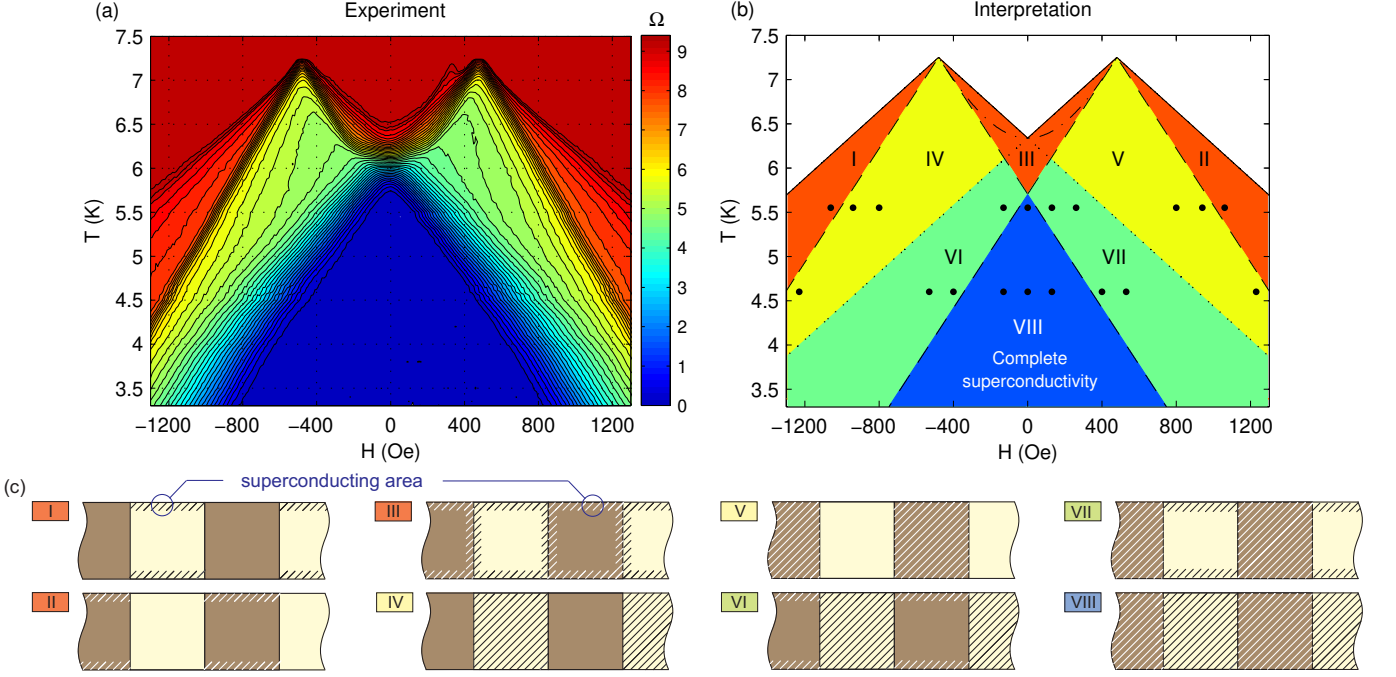


FIG. 6: (Color online) (a) Dc resistance R of the superconducting Pb bridge fabricated on top of the BFO crystal as a function of the external magnetic field H and temperature T at $I = 100 \mu\text{A}$. (b) Interpretation of the measured $R(H, T)$ dependence: solid lines describe the appearance of the edge-assisted reverse-domain superconductivity (EA-RDS), Eq. (5); dashed lines correspond to the appearance of reverse-domain superconductivity (RDS) and parallel-domain superconductivity (PDS), Eqs. (2)–(3); dotted lines describe the formation of edge-assisted parallel-domain superconductivity (EA-PDS); while black dash-dotted line describes the appearance of domain-wall superconductivity (DWS), Eq. (6). Here we used the following fitting parameters: $T_{c0} = 7.25 \text{ K}$, $B_0 = 480 \text{ Oe}$, and $H_{c2}^{(0)} = 2.25 \text{ kOe}$. The black dots correspond to the low-temperature scanning laser microscopy images obtained at $T = 4.60 \text{ K}$ and $T = 5.70 \text{ K}$ and which are presented in Figs. 10–11, respectively. (c) Schematic presentation of the different regimes of inhomogeneous superconductivity in the considered system. Bright and dark areas correspond to positive and negative magnetic domains respectively, shaded areas depict the expected superconducting regions: I and II – EA-RDS above positive and negative magnetic domains, respectively; III – complex state consisting of DWS and EA-RDS; IV and V – bulk RDS above positive and negative domains, respectively; VI and VII – complex states consisting of RDS and EA-PDS above positive and negative domains, respectively; VIII – complete superconductivity in the entire sample, consisting of RDS and PDS.

normal state and the total volume of the bridge. We observe that in the developed RDS state R is not constant but slightly increases with $|H|$. This finding can be attributed to the external-field-induced shrinkage of the reverse domains. However, even when bulk RDS is suppressed, the resistance is still lower than the normal resistance. Such a resistive state observed at low temperature and high field, can be attributed to the formation of compensated superconductivity above magnetic domains of opposite polarity but localized near the edge of the sample. In the following, this state will be referred to as edge-assisted RDS. Apparently, such states can exist until the local magnetic field above the opposite domains $|H - B_0|$ exceeds the critical field of surface superconductivity $H_{c3} = 1.69H_{c2}$ at a given temperature.^{36,37} The position of the critical fields $|H_{c2} + B_0|$ and $|H_{c3} + B_0|$, which determine the shape of the magnetoresistive curve, are shown in Fig. 5(b) for $T = 6.10 \text{ K}$. For instance, the

experimentally determined ratio H_{c3}/H_{c2} for $T = 6.10 \text{ K}$ is close to 1.77, supporting our interpretation.

H – T diagram. A full $H - T$ diagram for the long bridge, composed from isothermal $R(H)$ measurements, is presented in Fig. 6(a). A similar diagram for the short bridge is not given since both S/F hybrid samples showed almost identical behavior. The interpretation of all distinctive regions of this diagram is given in Fig. 6(b).

We explain the initial deviation of the resistance from the normal value R_n by the formation of the edge-assisted RDS for large H . Such states I and II are shown schematically in Fig. 6(c). For moderate H , superconductivity can appear in the form of a complex state consisting of edge-assisted superconductivity and DWS (pattern III). According to our expectations, the localized superconductivity in the latter case ($|H| < B_0$) appears above the phase transition line depicted by Eq. (6), since the

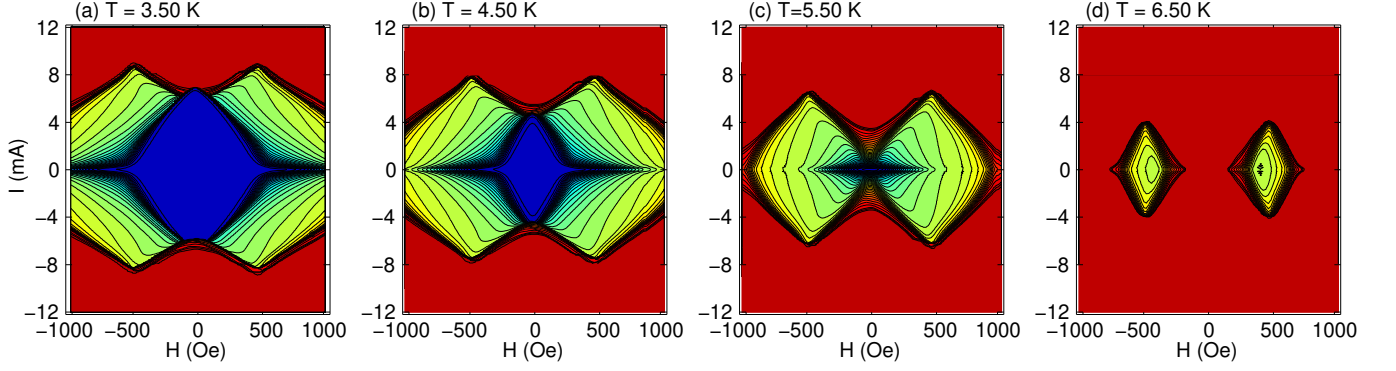


FIG. 7: (Color online) Dc resistance $R = V/I$ dependence of the long superconducting Pb bridge on the external magnetic field H and the bias current I taken at different temperatures: $T = 3.50$ K (a), $T = 4.50$ K (b), $T = 5.50$ K (c), and $T = 6.50$ K (d). We use the same color scheme as in Fig. 6(a).

critical temperature for DWS induced by the domain walls of a finite width should be always higher than that for infinitely narrow domain walls. Interestingly, in the overcompensated regime ($|H| > B_0$), the position of the shifted H_{c3} line, Eq. (5), coincides with the level curve $R(H, T) = 0.98 R_n$. The next stages of decreasing resistance with decreasing temperature at $|H| \sim B_0$ have to be associated with the appearance of bulk RDS in the compensated regions (patterns IV and V). The corresponding phase boundaries are given by Eqs. (2)–(3) and are shown by black dashed lines in Fig. 6(b). For temperatures below the transition line given by Eq. (5), in addition to RDS inhomogeneous superconductivity in the form of edge-assisted PDS also appears in the regions with enhanced magnetic field (patterns VI and VII). Inside the region VIII in the $H - T$ diagram, where areas of inhomogeneous superconductivity for the different domains start to overlap, the total absence of electrical resistance indicates the appearance of CS.

Thus, in our transport measurements, we clearly observed the switching between different regimes of localized superconductivity upon variation of H and T .

Critical currents. A bias current I can suppress the different modes of nonuniform superconductivity in the considered S/F system in various ways. The effect of H and I on the current (I) – voltage (V) dependencies and on the dc resistance $R = V/I$ are illustrated in Figs. 7 and 8. We observed that the state of RDS is more robust with respect to current injection than the state of CS, since in the latter case the bias current can first destroy the weakly-developed superconductivity above parallel magnetic domains (i.e., above positive domains at $H > 0$ and vice versa), where the local magnetic field is maximal.

In order to evaluate the critical current destroying CS and RDS, we consider the effect of T on the $I - V$ dependencies (Fig. 8) measured at $H = 0$ and $|H| \simeq B_0$ (i.e. close to the compensation field). One can see that the state with zero resistance, which is inherent to CS, can be destroyed if I exceeds a threshold value I_c^{CS} . Taking

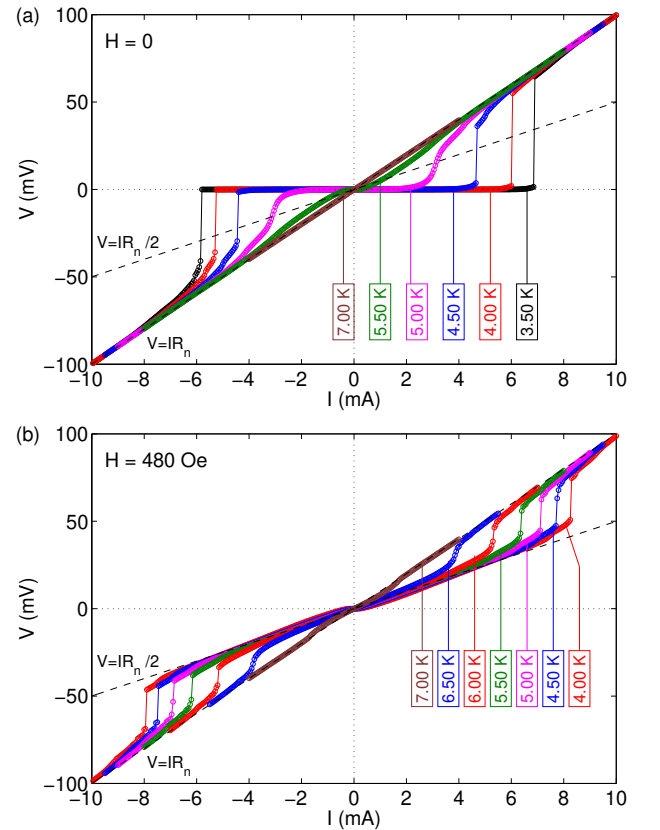


FIG. 8: (Color online) Typical $I - V$ dependencies measured at $H = 0$ (a) and $H = 480$ Oe (b) for the long superconducting Pb bridge at different temperatures indicated in the plots. Two dashed lines correspond to the Ohmic-like behavior with the resistance $R = R_n/2$ and $R = R_n$.

the position of the jumps in the $I - V$ curves at $H = 0$ or the maximal differential resistance dR/dH (panel (a) in Fig. 8), we plotted the temperature dependence of the critical current I_c^{CS} , corresponding to the destruction of the most developed CS state at $H = 0$. For a charac-

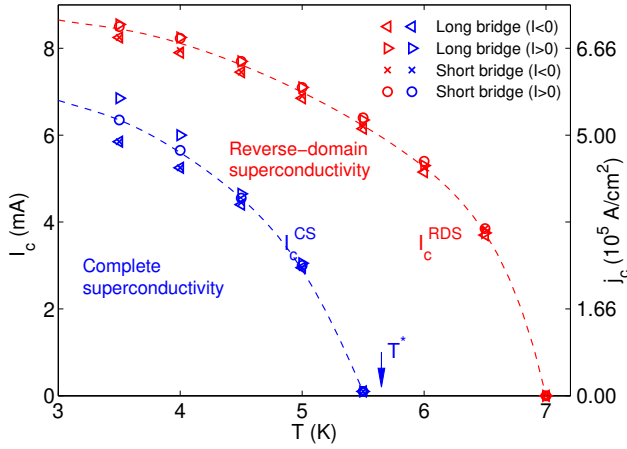


FIG. 9: (Color online) Temperature dependence of the critical currents I_c^{RDS} and I_c^{CS} , corresponding to the suppression of reverse-domain superconductivity (red symbols near the top line), and complete superconductivity (blue squares near the bottom line), respectively. For the determination of I_c^{RDS} (I_c^{CS}) we plotted the positions of the maximal differential resistance on the $I - V$ dependencies measured at $H = 480$ Oe ($H = 0$) both for the long and short bridges; $I < 0$ and $I > 0$ denote the negative and positive branches of the corresponding $I - V$ curves (Fig. 8). The dashed lines are guides to the eyes.

terization of the critical current I_c^{RDS} , corresponding to the suppression of the developed RDS at the compensation field ($|H| \simeq B_0$), we traced the position of the jump on the $I - V$ curves at $H = 480$ Oe upon increasing T (panel (a) in Fig. 8). Indeed, this estimate seems to be reasonable for the describing of the current-induced destruction of inhomogeneous superconductivity under the condition when the minimal resistance of the investigated sample in the superconducting state is finite (of the order of $50\%R_n$). The dependencies of the both estimated critical currents I_c^{RDS} and I_c^{CS} as a function of T are presented in Fig. 9.

IV. VISUALIZATION OF NONUNIFORM SUPERCONDUCTING STATES BY SCANNING LASER MICROSCOPY

In order to image the inhomogeneous superconducting states trapped by the nonuniform magnetic field we used low-temperature scanning laser microscopy (LTSLM).

The principle of operation of LTSLM can be introduced as follows.^{9,40–43} The hybrid S/F samples were mounted on the cold finger of a Helium gas flow cryostat, which is equipped with optical windows to enable laser irradiation. An amplitude modulated laser beam (wave length 680 nm, modulation frequency 10 kHz) heats locally the superconducting sample within a spot with a diameter of $1.5 - 2 \mu\text{m}$. This value is determined by the diameter of the focused incident beam and by the thermal conductivity of the tested bilayer sample.⁴¹ The incident beam

intensity power on the sample surface (up to $\sim 25 \mu\text{W}$) appears to be high enough to provide a maximum beam-induced increase in temperature $\Delta T \sim 0.1 - 0.2$ K, leading to a local suppression of superconductivity within this hot spot. We assume that the effect of the laser irradiation should be uniform across the superconducting film thickness since the thickness of the Pb film (40 nm) is much smaller than the lateral spot size. In our LTSLM measurements we apply a constant bias current and measure the beam-induced voltage drop ΔV along the entire bridge by lock-in technique. A set of scanning mirrors allows us to control the position (x, y) of the spot and thus, to obtain the position-dependent 2D map of the LTSLM signal: $\Delta V = \Delta V(x, y)$.

The LTSLM voltage signal can be interpreted as follows. If the laser spot heats an area of the bridge which is in the normal resistive state, the beam-induced perturbation of the local temperature causes only a very small change in the total resistance, since $\partial R_n / \partial T$ is very small. However, if the irradiated part of the bridge is in the superconducting state and it took part in the transfer of a substantial part of the supercurrents, the beam-induced suppression of superconductivity might switch the whole sample from a low-resistive state to a high-resistive state. In other words, the LTSLM technique makes it possible to map out the ability of the sample to carry supercurrents. Comparing the LTSLM responses upon varying H and T , one can trace the evolution of local superconducting properties in the investigated system.

For the observation of the different regimes of inhomogeneous superconductivity in the long Pb/BFO hybrid samples, we applied a constant current of $I = 300 \mu\text{A}$ and the field was varied in the range between $H = \pm 1350$ Oe.

Figure 10 shows the LTSLM images obtained at $T = 4.60$ K, which is below the crossover temperature $T^* = 5.70$ K. For $|H| \leq 130$ Oe the measured responses have no detectable variations [see panels (a), (b1) and (b2)]. Apparently, at these points inside the CS state in the $H - T$ diagram, the intensity of the laser beam is insufficient for the destruction of the developed bulk superconductivity.

According to our estimates, at $T = 4.60$ K, the depletion of superconductivity above the parallel magnetic domains should occur at $|H| \gtrsim 350$ Oe. This means that near the “CS-RDS” transition line the areas above the parallel domains have to be in the *resistive* state, while the areas above the opposite domains are still in the superconducting state. As a result, the maxima in the LTSLM response at $H = 400$ Oe should be attributed solely to the non-superconducting regions above the positive domains [panels (c2), (d2)]. Correspondingly, at $H = -400$ Oe the resistive areas above negative domains are responsible for the beam-induced voltage [panels (c1), (d1)]. At higher H values (i.e. deeper in the RDS areas in the $H - T$ diagram) superconductivity survives exclusively above the opposite domains and such compensated superconductivity is strong enough not to be destroyed by the laser beam of the given intensity. However, close to the transition

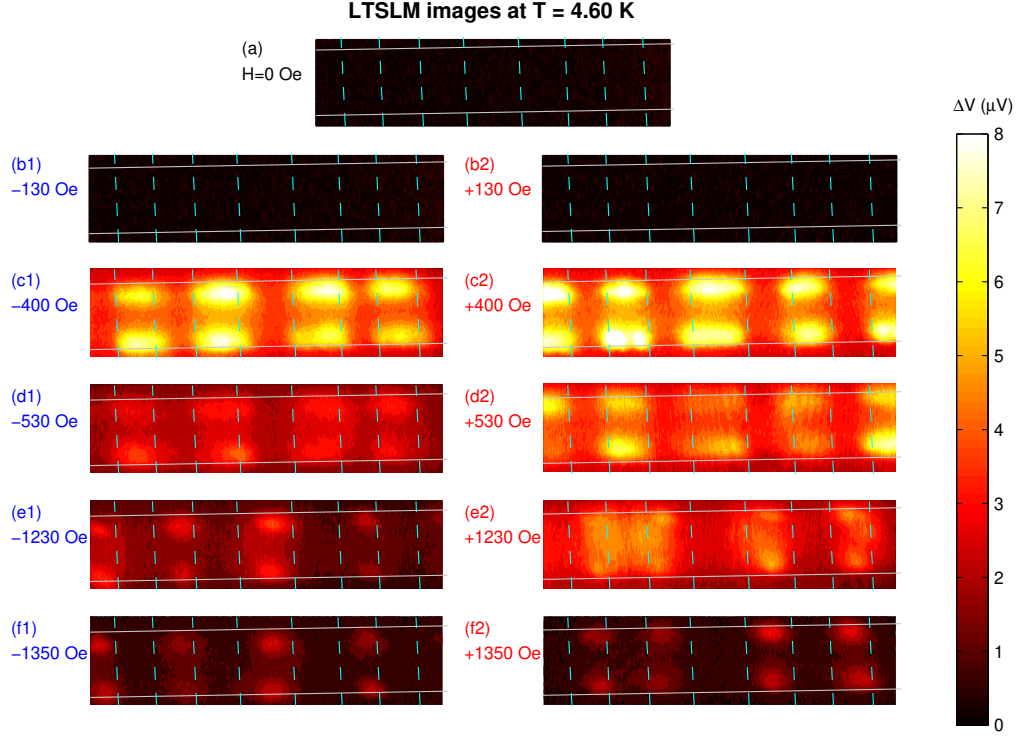


FIG. 10: (color online) Low-temperature scanning laser microscopy (LTSLM) images obtained for the same area of the long Pb bridge at $T = 4.60$ K. The color scale indicates the change in the beam-induced voltage drop ΔV . The H values are indicated in the plots and the bias points for all presented images are also marked by black dots in the phase diagram in Fig. 6(b). The scanning area is about $120 \mu\text{m} \times 40 \mu\text{m}$. Vertical dashed cyan lines indicate the positions of the domain walls. The sample edges are marked by horizontal solid white lines.

line “RDS – edge-assisted RDS” the reverse-domain superconductivity becomes weaker and can be affected by the laser beam. Therefore, the bright areas in the corresponding LTSLM signal originate from the regions with the compensated magnetic field above the opposite domains. The inversion of the H sign immediately results in a switching between enhanced reverse-domain superconductivity and depleted parallel-domain superconductivity for the same areas of the superconducting bridge [panels (e1–e2) and (f1–f2)]. Thus, all findings concerning the migration of the maximal beam-induced voltage along the Pb bridge upon varying H are in agreement with our transport measurements.

We would like to note that the LTSLM images [panels (c1–f1) and (c2–f2) in Fig. 10] reveal an inhomogeneity of the beam-induced voltage across the width of the bridge. Indeed, the ΔV maxima are always located near the edges of the bridge. At the present moment we have no reliable interpretation of this effect. Probably, it can be explained by the current enhancement near the sample edges, typical for plain superconducting bridges,^{44,45} or by a suppression of the energy barrier for flux entry or exit for superconductors in the developed mixed state. Another possible explanation for the pronounced edge signal is the manifestation of edge-assisted PDS, since

such edge-assisted PDS states seem to be the states with weakest superconductivity. Finally, the edge signal can be explained by a hampered heat diffusion and, correspondingly, a larger heating effect of the beam focused near the edges as compared to that in the interior of the bridge. In any case, this issue requires a detailed theoretical treatment which is beyond the scope of the present work.

At $T = 5.50$ K, close to the crossover temperature, a voltage signal can be detected at $H = 0$. The amplitude of the built-in magnetic field is close to the corresponding upper critical field and therefore even a weak optical influence can substantially suppress bulk superconductivity equally above the domains of both polarities. Upon increasing $|H|$ we successively observe the responses from the parallel domains [panels (b1) and (b2–c2)] and from the antiparallel domains [panels (d1–f1) and (d2–f2)], similar to that described above.

Further increase in temperature above the crossover temperature could allow us to detect the domain-wall superconductivity at $H = 0$, since the masking background signal from CS and the edge-assisted RDS are turned off. The evolution of the beam-induced voltage upon increasing T is presented in Fig. 12, where we show line scans $\Delta V(x)$ along the bridge, close to the bottom

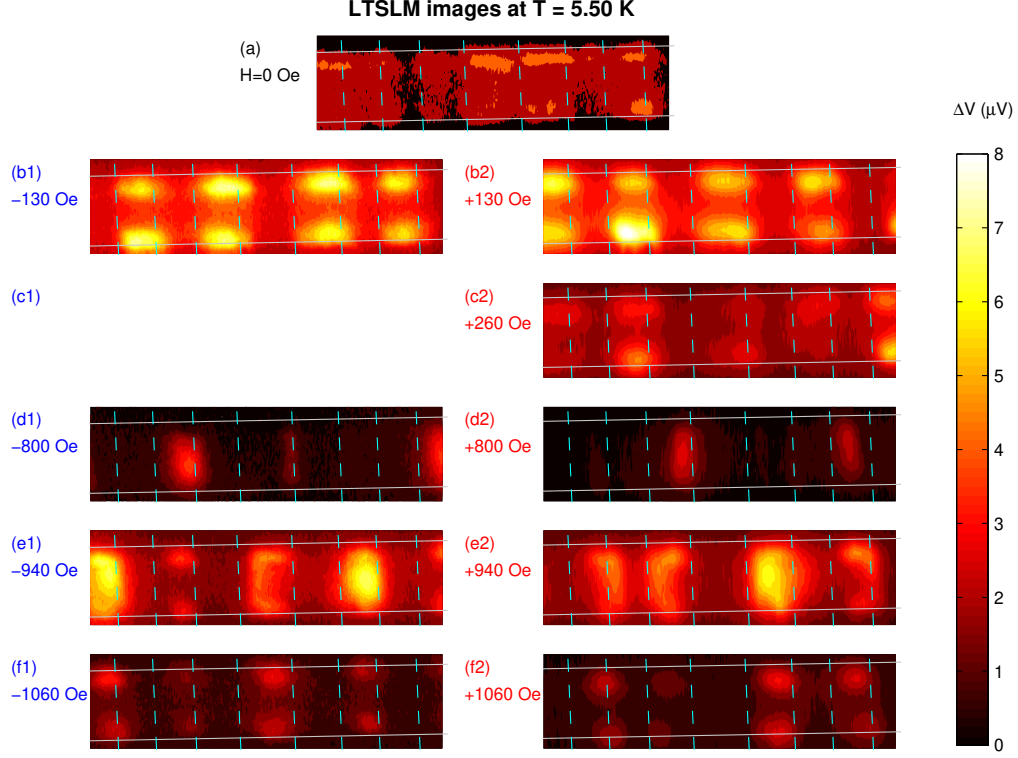


FIG. 11: (color online) Low-temperature scanning laser microscopy (LTSLM) images obtained for the same area of the long Pb bridge at $T = 5.50$ K. All parameters and notations are the same as in Fig. 10. The LTSLM image at $H = -260$ Oe (panel (c1)) was recorded with technical problems and therefore we do not present this plot.

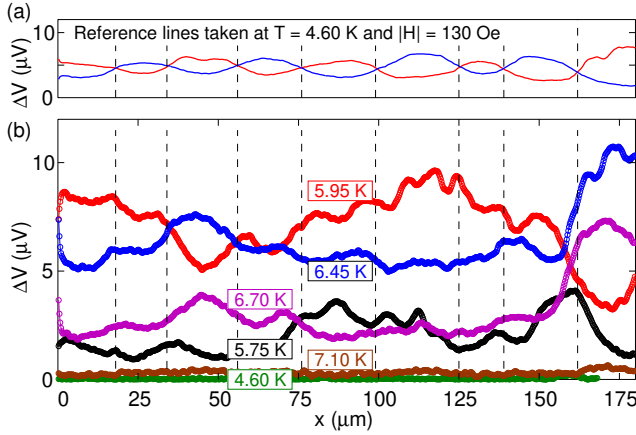


FIG. 12: (color online) Line scans $\Delta V(x)$ obtained by LTSLM method at different T along the line close to the lower edge of the Pb microbridge: (a) the reference signal $\Delta V(x)$ measured at $H = \pm 130$ Oe in order to detect the positions of the domain walls shown as vertical dashed lines. (b) The dependencies $\Delta V(x)$ measured at different temperatures (shown in the plot) and $H = 0$.

edge of the bridge. We did not find any noticeable increase in the LTSLM response near the domain walls for

the considered S/F system. We would like to mention that the DWS state was observed for a similar Pb bridge oriented along the domain wall using the same LTSLM technique.⁴⁶

V. CONCLUSION

We presented a detailed experimental study of the superconducting properties of thin-film superconducting Pb microbridges in the presence of a nonuniform magnetic field of the laminar domain structure in ferromagnetic $\text{BaFe}_{12}\text{O}_{19}$ crystals. Such ferromagnets generate rather strong stray fields and the parameters of this field (amplitude and period) are almost independent on the applied magnetic field H in the considered H range. We focused on the case when the domain walls are oriented perpendicular to the bridge in order to avoid electrical shunting and masking of less developed superconducting states by more favorable states during transport measurements. It was demonstrated that, at high temperatures superconductivity appears in the form of reverse-domain superconductivity only above magnetic domains of opposite polarity with respect to the H sign. Below the crossover temperature T^* , defined as $H_{c2}(T^*) = B_0$, superconductivity can nucleate both above antipar-

allel and parallel magnetic domains (B_0 is the amplitude of the perpendicular component of the nonuniform field, $H_{c2} = H_{c2}^{(0)} (1 - T/T_{c0})$ is the temperature-dependent upper critical field). Indeed, at $T < T^*$ the regions of inhomogeneous superconductivity above positive and negative domains overlap in the $H - T$ plane, resulting in so-called complete (or global) superconductivity and in the vanishing total electrical resistance of the hybrid sample. We also found experimental evidences for the regimes of edge-assisted reverse-domain superconductivity and edge-assisted parallel-domain superconductivity, corresponding to localized superconductivity near the edges of the bridge above the regions with compensated and enhanced magnetic field, respectively. We experimentally determined the critical currents, corresponding to the suppression of the localized superconductivity above parallel and antiparallel magnetic domains in a broad temperature range. The technique of low-temperature scanning laser microscopy made it possible to directly visualize the temperature- and field-induced

transitions from complete superconductivity to reverse-domain superconductivity and parallel-domain superconductivity and from these inhomogeneous superconducting states to the normal state.

VI. ACKNOWLEDGEMENTS

This work was supported by the Methusalem Funding of the Flemish Government, the NES – ESF program, the Belgian IAP, the Fund for Scientific Research – Flanders (F.W.O.–Vlaanderen), the Russian Fund for Basic Research, RAS under the Program “Quantum physics of condensed matter”, Russian Agency of Education under the Federal Target Program “Scientific and educational personnel of innovative Russia in 2009–2013”, Deutsche Forschungsgemeinschaft (DFG) via grant no. KO 1303/8-1. Robert Werner acknowledges support by the Cusanuswerk, Bischöfliche Studienförderung.

-
- ¹ A.I. Buzdin, Rev. Mod. Phys. **77**, 935 (2005).
 - ² I.F. Lyuksyutov and V.L. Pokrovsky, Adv. Phys. **57**, 67 (2005).
 - ³ M. Vélez, J.I. Martín, J.E. Villegas, A. Hoffmann, E.M. González, J.L. Vicent, and I.K. Schuller, Journ. Magn. Magn. Mater. **320**, 2547–2562 (2008).
 - ⁴ A.Yu. Aladyshkin, A.V. Silhanek, W. Gillijns, and V.V. Moshchalkov, Supercond. Sci. Technol. **22**, 053001 (2009).
 - ⁵ W. Gillijns, A.Yu. Aladyshkin, M. Lange, M.J. Van Bael, and V.V. Moshchalkov, Phys. Rev. Lett. **95**, 227003 (2005).
 - ⁶ W. Gillijns, A.Yu. Aladyshkin, A.V. Silhanek, and V.V. Moshchalkov, Phys. Rev. B **76**, 060503(R) (2007).
 - ⁷ A.Yu. Aladyshkin, A.P. Volodin, V.V. Moshchalkov, J. Appl. Phys. **108**, 033911 (2010).
 - ⁸ Z. Yang, M. Lange, A. Volodin, R. Szymczak, and V.V. Moshchalkov, Nature Mater. **3**, 793 (2004).
 - ⁹ J. Fritzsche, V.V. Moshchalkov, H. Eitel, D. Koelle, R. Kleiner, and R. Szymczak, Phys. Rev. Lett. **96**, 247003 (2006).
 - ¹⁰ Z. Yang, J. van de Vondel, W. Gillijns, W. Vinckx, V.V. Moshchalkov, and R. Szymczak, Appl. Phys. Lett. **88**, 232505 (2006).
 - ¹¹ Z. Yang, K. Vervaeke, V.V. Moshchalkov, and R. Szymczak, Phys. Rev. B **73**, 224509 (2006).
 - ¹² A.Yu. Aladyshkin, J. Fritzsche, and V.V. Moshchalkov, Appl. Phys. Lett. **94**, 222503 (2009).
 - ¹³ A.Yu. Aladyshkin, J. Fritzsche, and V.V. Moshchalkov, Physica C, Physica C **470**, 883 (2010).
 - ¹⁴ A.Yu. Aladyshkin, D.Yu. Vodolazov, J. Fritzsche, R.B.G. Kramer and V.V. Moshchalkov, Appl. Phys. Lett. **97**, 052501 (2010).
 - ¹⁵ L.Y. Zhu, T.Y. Chen, and C.L. Chien, Phys. Rev. Lett. **101**, 017004 (2008).
 - ¹⁶ L.Y. Zhu, Marta Z. Cieplak, and C.L. Chien, Phys. Rev. B **82**, 060503(R) (2010).
 - ¹⁷ S. Haindl, M. Weisheit, T. Thersleff, L. Schultz and B. Holzapfel, Supercond. Sci. Technol. **21**, (2008) 045017.
 - ¹⁸ J. Fritzsche, R.B.G. Kramer, and V.V. Moshchalkov, Phys. Rev. B **80**, 094514 (2009).
 - ¹⁹ V.K. Vlasko-Vlasov, U. Welp, A. Imre, D. Rosenmann, J. Pearson, and W.K. Kwok, Phys. Rev. B **78**, 214511 (2008).
 - ²⁰ V. Vlasko-Vlasov, U. Welp, G. Karapetrov, V. Novosad, D. Rosenmann, M. Iavarone, A. Belkin, and W.-K. Kwok, Phys. Rev. B **77**, 134518 (2008).
 - ²¹ V. Vlasko-Vlasov, U. Welp, W. Kwok, D. Rosenmann, H. Claus, A.A. Buzdin, and A. Melnikov, Phys. Rev. B **82**, 100502(R) (2010).
 - ²² C. Bell, S. Tursucu, and J. Aarts, Phys. Rev. B **74**, 214520 (2006).
 - ²³ R. K. Rakshit, R. C. Budhani, T. Bhuvana, V. N. Kulkarni, and G. U. Kulkarni, Phys. Rev. B **77**, 052509 (2008).
 - ²⁴ R. K. Rakshit, S. K. Bose, R. Sharma, N. K. Pandey, and R. C. Budhani, Phys. Rev. B **77**, 094505 (2008).
 - ²⁵ A. Belkin, V. Novosad, M. Iavarone, J. Fedor, J. E. Pearson, A. Petrean-Troncalli, and G. Karapetrov, Appl. Phys. Lett. **93**, 072510 (2008).
 - ²⁶ A. Belkin, V. Novosad, M. Iavarone, J. Pearson, and G. Karapetrov, Phys. Rev. B **77**, 180506 (2008).
 - ²⁷ G. Karapetrov, M. V. Milošević, M. Iavarone, J. Fedor, A. Belkin, V. Novosad, and F. M. Peeters, Phys. Rev. B **80**, 180506 (2009).
 - ²⁸ A. Belkin, V. Novosad, M. Iavarone, R. Divan, J. Hiller, T. Proslir, J. E. Pearson, and G. Karapetrov, Appl. Phys. Lett. **96**, 092513 (2010).
 - ²⁹ C. Visani, N.M. Nemes, M. Rocci, Z. Sefrioui, C. Leon, S.G.E. te Velthuis, A. Hoffmann, M. R. Fitzsimmons, F. Simon, T. Feher, M. Garcia-Hernandez, and J. Santamaria, Phys. Rev. B **81**, 094512 (2010).
 - ³⁰ T. Tamegai, Y. Nakao, S. Mohan and Y. Nakajima, Supercond. Sci. Technol. **24**, 024015 (2011).
 - ³¹ B. Pannetier, S. Rodts, J.L. Genicon, Y. Otani and J.P. Nozières, chapter in *Macroscopic Quantum Phenomena and Coherence in Superconducting Networks*, Eds. C. Gio-

- vannella and M. Tinkham, (Singapore: World Scientific), pp. 17–24 (1995).
- ³² M. Lange, M.J. Van Bael, Y. Bruynseraede, and V.V. Moshchalkov, Phys. Rev. Lett. **90**, 197006 (2003).
- ³³ A.Yu. Aladyshkin, A.I. Buzdin, A.A. Fraerman, A.S. Mel'nikov, D.A. Ryzhov, A.V. Sokolov, Phys. Rev. B **68**, 184508 (2003).
- ³⁴ A.Yu. Aladyshkin and V.V. Moshchalkov, Phys. Rev. B **74**, 064503 (2006).
- ³⁵ A.I. Buzdin and A.S. Mel'nikov, Phys. Rev. B **67**, 020503(R) (2003).
- ³⁶ D. Saint-James, G. Sarma, E.J. Thomas, *Type-II superconductivity* (Pergamon Press, 1969).
- ³⁷ M. Tinkham, *Introduction to Superconductivity* (2nd ed., McGraw-Hill Inc., 1996).
- ³⁸ Equation (6) may be considered as an ultimate estimate of DWS, since the critical temperature of the solution, localized in vicinity of the domain walls of the finite width, will be always higher than that given by Eq. (6).
- ³⁹ S.J. Bending, Adv. Phys. **48**, 449 (1999).
- ⁴⁰ L.R. Testardi, Phys. Rev. B **4**, 2189 (1971).
- ⁴¹ J. Fritzsche, Ph.D. thesis, Katholieke Universiteit Leuven (2008).
- ⁴² M. Wagenknecht, H. Eitel, T. Nachtrab, J. B. Philipp, R. Gross, R. Kleiner, and D. Koelle, Phys. Rev. Lett. **96**, 047203 (2006).
- ⁴³ H. B. Wang, S. Guénon, J. Yuan, A. Iishi, S. Arisawa, T. Hatano, T. Yamashita, D. Koelle, and R. Kleiner, Phys. Rev. Lett. **102**, 017006 (2009).
- ⁴⁴ M.Yu. Kupriyanov, K.K. Likharev, Fiz. Tverd. Tela **16**, 2829 (1974) [Sov. Phys. – Solid State **16**, 1835 (1975)].
- ⁴⁵ A.A. Elistratov, D.Yu. Vodolazov, I.L. Maksimov, and J.R. Clem, Phys. Rev. B **66**, 220506 (2002).
- ⁴⁶ R. Werner, A.Yu. Aladyshkin, S. Guénon, J. Fritzsche, I.M. Nefedov, V.V. Moshchalkov, R. Kleiner, and D. Koelle, submitted (2011).